Applied Catalysis B: Environmental 218 (2017) 819–824

Contents lists available at ScienceDirect

Applied Catalysis B: Environmental

journal homepage: www.elsevier.com/locate/apcatb

Synergistic combination of bandgap-modified carbon nitride and WO_3 for visible light-induced oxidation of arsenite accelerated by in-situ Fenton reaction

Gun-hee Moon, Sujeong Kim, Young-Jin Cho, Jonghun Lim, Dong-hyo Kim, Wonyong Choi *

Division of Environmental Science and Engineering & Department of Chemical Engineering, Pohang University of Science and Technology (POSTECH), Pohang 37673, Republic of Korea

ARTICLE INFO

Article history:
Received 23 April 2017
Received in revised form 3 July 2017
Accepted 9 July 2017
Available online 11 July 2017

Keywords:
Visible light photocatalysis
Carbon nitride
Tungsten oxide
In-situ Fenton reaction
Arsenic oxidation

ABSTRACT

Photocatalytic oxidation of arsenite (As(III)) to arsenate (As(V)) using non-toxic semiconductor materials has been considered as an environmentally-benign pretreatment process of arsenic contaminated waters, but poor visible light activity hinders the practical applications utilizing solar light. In this study, we designed a ternary photocatalytic system consisting of modified carbon nitride (mCN), WO_3, and Fe^{3+} for efficient oxidation of As(III) which was done by using *in-situ* generated H_2O_2 as a Fenton reagent under visible light ($\lambda > 420$ nm). While superoxide anion and H_2O_2 were effectively produced via the reduction of dissolved O_2 by mCN, WO_3 regenerated Fe^{2+} from Fe^{3+}, which activated *in-situ* generated H_2O_2 for Fenton process. The overall photocatalytic oxidation activity of As(III) was optimized at a specific mixing ratio of catalysts (mCN:WO_3 = 60:40) where there is an optimal balance between the conduction band electron transfer to dissolved O_2 (to produce H_2O_2 on mCN) and the competing electron transfer to Fe^{3+} (to regenerate Fe^{2+} on WO_3). The ternary combination enabled the simultaneous participation of superoxide anions, hydroxyl radicals, and holes to complete the oxidation of 500 μM As(III) within 90 min with 1.0 g/L catalyst and 70 μM Fe^{3+} and that of 10 μM As(III) within 60 min with a tenth amount of catalyst (0.1 g/L) and Fe^{3+} (7 μM) under visible light without requiring noble metal catalysts and chemical additives. The process consists of earth abundant elements only (C, N, O, W, and Fe) and operates with utilizing visible light photons and dissolved O_2 only, which is eco-friendly and cost effective.

1. Introduction

Arsenic (As) contamination of groundwater and soil induced by both natural and human activities has been a critical environmental issue threatening the human health [1–3]. To effectively remove As from contaminated water, the pre-oxidation process of arsenite (As(III)) to arsenate (As(V)) is highly desired because As(V) has lower toxicity, lower mobility, and higher affinity for adsorbents [4–6]. The pre-oxidation can be carried out by various advanced oxidation processes (AOPs) [7] among which the photocatalytic oxidation (PCO) has several advantages involving (i) no need of chemical oxidants except dissolved O_2, (ii) operation under natural sunlight and ambient conditions without needing extra power, (iii) strong photooxidation capability for a wide variety of contaminants (not limited to As(III)), and (iv) low cost and environmentally-benign nature of photoactive materials [8,9]. Recently, the PCO of As(III) was successfully achieved by hybridization of reduced graphene oxide (rGO) with TiO_2 (rGO/TiO_2), which exhibited a highly enhanced PCO activity comparable to platinum-deposited TiO_2 (Pt/TiO_2) [10]. However, the lack of the visible light activity of the titania-based materials limits its solar applications [10,11]. Although a few photocatalysts (Pd-modified N-doped TiO_2 [12], V_2O_5/TiO_2 [13], BiOI [14], $Bi_2Sn_2O_7$ [15], Pt/WO_3 [16], etc.) with visible light activity have been reported for the PCO of As(III), most studies were focused on materials preparation and characterization and little was done on detailed photoactivity assessment and mechanistic analysis. It should be also noted that an efficient photocatalytic system can be achieved not only by the development of new materials but also by the elaborate design of new reaction pathways using a combination of known catalytic materials.

In this study, we propose a hybrid photocatalytic system consisting of modified carbon nitride (mCN), tungsten oxide (WO_3),

* Corresponding author.
E-mail address: wchoi@postech.edu (W. Choi).

http://dx.doi.org/10.1016/j.apcatb.2017.07.021
0926-3373/

and ferric (Fe^{3+}) ions, which utilizes *in-situ* generated H_2O_2 as a Fenton reagent for efficient oxidation of As(III) under visible light (λ > 420 nm). Typical Fenton reactions utilize externally added H_2O_2 as a reagent, which is responsible for the main cost of Fenton process. Therefore, *in-situ* generation of H_2O_2 via O_2 reduction would be an economically ideal option for practical Fenton processes. The photocatalytic production of H_2O_2 via O_2 reduction has been recently demonstrated using rGO/TiO_2 [17] and modified CN [18,19]. In particular, CN (also commonly referred as *graphitic* CN) has been reported as an efficient photocatalyst for the production of H_2O_2 under visible light irradiation since tri-s-triazine moieties facilitated two electron transfer to dissolved O_2, involving the sequential formation of superoxo radical and 1,4-endoperoxide intermediates [20]. Moreover, the modification of the CN polymeric structure by pyromellitic diimide (PDI) further increased the production of H_2O_2 [18,21]. Although a few studies have investigated the photocatalytic production of H_2O_2 [22–24], the utilization of *in-situ* generated H_2O_2 as a Fenton reagent for the oxidation of water contaminants has not been reported. This study proposed a hybrid photocatalytic system consisting of *in-situ* generation of H_2O_2 and the subsequent regenerative Fenton process, which was enabled by the synergic combination of mCN and WO_3. WO_3 is a good visible light photocatalyst [16,25] that can be combined with CN owing to the suitable band edge positions relative to those of CN, good stability at acidic and neutral pH, and non-toxicity of material. The proposed system successfully operates with utilizing visible light photons and dissolved O_2 only for the efficient oxidation of As(III).

2. Experimental section

2.1. Synthetic methods

Melem was prepared by thermal condensation of melamine (Aldrich) at 425 °C for 4 h, followed by refluxing at 100 °C for several hours, washing, and drying. The melem was uniformly mixed with pyromellitic diimide (PDI, Aldrich) with a different molar ratio (mCN (1:1), mCN-1 (1:2), and mCN-2 (1:3)). The mixture in a porcelain crucible covered with a lid was calcined at 325 °C for 4 h. The detailed experimental procedure was well described in the literature [18,21]. The product was ground, dispersed in aqueous medium, and sonicated for 1 h. The yellow suspension was filtered, washed, and dried at room temperature. Unmodified CN was prepared by heat treatment of melamine at 550 °C for 4 h. WO_3 (nanopowder, <100 nm particle size) was purchased from Sigma-Aldrich.

2.2. Materials characterizations

The diffuse reflectance UV/Visible spectra (DRUVS) for CN and mCN were obtained by a spectrophotometer (Agilent 8453). Infrared spectra of CN and mCN were recorded by Attenuated total reflectance Fourier transform infrared spectroscopy (ATR-FTIR, Thermo Scientific iS50) using ZeSe crystal. X-ray diffraction (XRD) patterns for CN, mCN, and WO_3 were measured by a PANalytical X'Pert diffractometer with an X'Celerator detector using Cu K_a line (1253.6 eV). X-ray photoelectron spectroscopy (XPS) VB analysis for CN and mCN was performed by ESCALAB 250 XPS System (Thermo Fisher Scientific, UK) with an X-ray source using monochromatic Al Kα (1486.6 eV). The spectra were corrected by Au 4f (84.0 eV) peak. Photoluminescence (PL) emission spectra were recorded by a fluorescence spectrometer (Shimadzu RF-5301), and the experimental procedure for measuring time-resolved PL (TRPL) was the same as described in a previous paper [19]. The nitrogen adsorption/desorption isotherms were obtained using Tristar II 3020 (Micromeritics Instrument Corporation). The transmission electron microscopy (TEM) images were obtained by JOEL JEM-2200FS. To avoid similar explanations that were already mentioned in previous studies, the interpretations and discussion about the characterization data of pure CN and mCN are briefly described in the supplementary data (*see* Figs. S1–S7).

2.3. Photo-activity measurements

Total 40 mg of the samples was dispersed in purified water (38 mL) by ultra-sonication and 2 mL of 10 mM sodium arsenite ($NaAsO_2$, Aldrich) solution was added to fix the concentration of As(III) at 500 μM. The mass ratio of WO_3 to mCN was gradually increased with the total catalyst (mCN + WO_3) mass fixed at 40 mg. After adding ferric ions, the pH of the suspension was adjusted at pH 3 by $HClO_4$ to avoid the formation of iron hydroxides. Before irradiation, it was stirred in dark for 30 min to pre-adsorb As(III) under O_2 saturated conditions. The reactor was irradiated by a 300-W Xe arc lamp (Oriel) under continuous stirring and O_2 purging. Light was passed through a 10-cm IR filter and a cutoff filter (λ ≥ 420 nm), and then was focused onto the reactor. For Ar-saturated condition, the reactor was tightly sealed and purged with high purity Ar gas before and during the irradiation. To double check the effect of radical scavengers, 500 mM *tert*-butyl alcohol (TBA, Aldrich) or 20 mM benzoic acid (BA, Aldrich) was added as a hydroxyl radical scavenger, and 20 mM benzoquinone (BQ) or superoxide dismutase (SOD) was used as a superoxide anion scavenger. The concentration of As(V) and hydrogen peroxide and the slurry-type photocurrent were measured using the same method as described in our previous work [10]. The concentration of ferric ions was measured by the spectrophotometric determination of Fe-1,10 phenanthroline complex.

3. Results and discussion

3.1. Photocatalytic production of H_2O_2

Fig. S8 compares the photocatalytic production of H_2O_2 in O_2-saturated suspension with different contents of PDI in CN under visible light irradiation (λ > 420 nm). While the production of H_2O_2 with pure CN was negligible, the introduction of PDI significantly increased the photocatalytic efficiency, which is consistent with a previous study [18]. In this study, the highest activity of mCN was observed when the mass ratio of PDI to melem was 1:1 and this optimized mCN was chosen as a main catalyst for this study. WO_3 was added as the second photocatalyst component to facilitate the conversion of Fe^{3+} to Fe^{2+} for a regenerative Fenton process. Although the reduction potential ($E^o(Fe^{3+}/Fe^{2+}) = 0.77$ V) is suitable to accept conduction band (CB) electrons from both mCN and WO_3, it turned out that the ferric-ferrous conversion is preferred on WO_3, which will be discussed later. To test the effect of WO_3 content on the photocatalytic production of H_2O_2, the mass of WO_3 added to the catalyst suspension (with the total catalyst (mCN + WO_3) concentration fixed at 1 g/L) was gradually increased (Fig. 1a). The photocatalytic production of H_2O_2 decreased with increasing the WO_3 content in the mixed catalysts suspension and was negligible in the suspension of 100% WO_3. The result indicates that H_2O_2 is produced only on mCN part (*not on WO_3 at all*). This is understandable because the CB edge position of WO_3 (+0.3 to 0.5 V_{NHE}) [16] is not energetically favorable to reduce O_2 [$E^0(O_2/O_2^{-\bullet}) = -0.33$ V_{NHE} and $E^0(O_2/HO_2^{\bullet}) = -0.05$ V_{NHE}] [26]. In addition, it should be noted that the production of H_2O_2 linearly decreased as the mCN content decreased (or as the WO_3 content increased) (Fig. 1b). This implies that *in-situ* generated H_2O_2 is not decomposed on the surface of WO_3 because the photocatalytic decomposition of H_2O_2 on WO_3, if it had occurred, would have decreased the production of H_2O_2 in

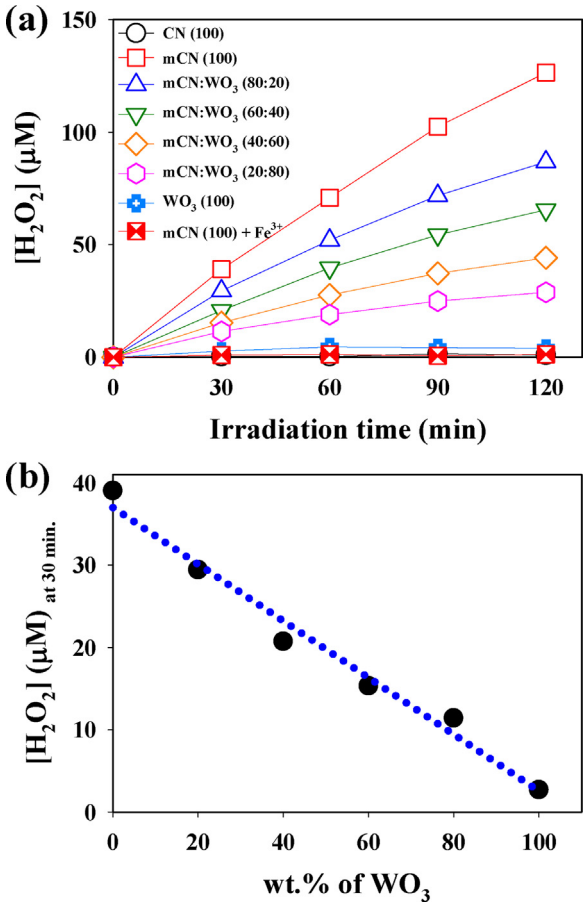

Fig. 1. (a) Comparison of the photocatalytic production of H_2O_2 in pure and mixed suspensions of mCN and WO_3. (b) WO_3 content-dependent production of H_2O_2 in the mixture suspension of mCN and WO_3 after 30 min irradiation. The experimental conditions were: [cat.] = 1.0 g/L, [Fe^{3+}] = 70 μM, pH_i = 3, continuous O_2-purging, and λ > 420 nm.

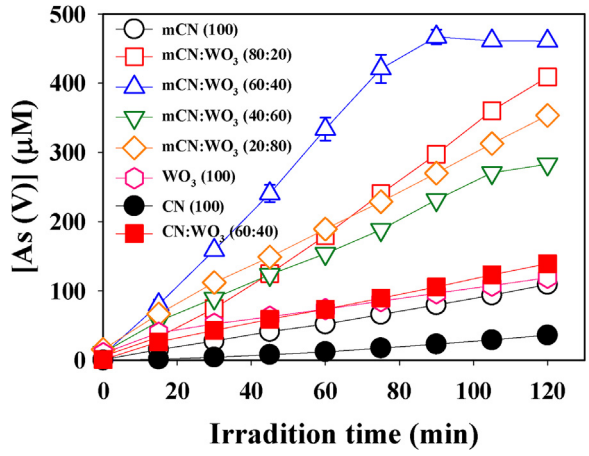

Fig. 2. Photocatalytic oxidation of As(III) in pure and mixed suspensions of mCN and WO_3 in the presence of Fe^{3+}. The experimental conditions were: [cat.] = 1.0 g/L, $[As(III)]_0$ = 500 μM, [Fe^{3+}] = 70 μM, pH_i = 3, continuous O_2-purging, and λ > 420 nm.

the mixed suspension of mCN and WO_3 more rapidly (*not linearly*) as the WO_3 content increased [27].

The decomposition of H_2O_2 seems to be mainly induced by its reaction with ferric/ferrous ions since the photocatalytic formation of H_2O_2 in mCN suspension was completely prohibited in the presence of ferric ions (*see* Fig. 1a). Since the VB potential of mCN is more negative than the potential for hydroxyl radical generation ($E^0(^\bullet OH/H_2O) = 2.7\ V_{NHE}$) [9,18], the OH radical generation by direct hole transfer on mCN should not be considered (*see* the energy level diagram in Scheme 1). As Fenton reaction should generate OH radicals, the enhanced generation of hydroxyl radicals was observed in mCN suspension when ferric ions were added as shown in Fig. S9: the generation of OH radical was indirectly monitored by detecting 7-hydroxycoumarin (7-HC) which is produced from the PCO reaction between OH radical and coumarin (coumarin + $^\bullet OH \rightarrow$ 7-HC) [28]. Since both O_2 and Fe^{3+} are competing for CB electrons [29], an excessive addition of Fe^{3+} should decrease the formation of H_2O_2 and consequently the formation of hydroxyl radicals. In addition, excessive Fe^{3+} ions can serve as a charge recombination center with making null cycles [30]. Therefore, the generation of OH radicals was optimized at [Fe^{3+}] = 70 μM, which was employed in further experiments.

3.2. Photocatalytic oxidation of arsenite

The positive role of WO_3 is clearly shown in its effect on the PCO of As(III) (Fig. 2). mCN alone or WO_3 alone exhibited low PCO activities but their mixture synergically enhanced the PCO efficiency, which was optimized at the mixture ratio of 60:40 (mCN:WO_3). Further increase of the WO_3 content above 40% reduced the overall PCO activity. As a control experiment, the unmodified CN was also tested and it exhibited the lowest PCO activity and the addition of WO_3 to unmodified CN slightly enhanced the PCO activity. Although the production of H_2O_2 was the largest in pure mCN suspension, the As(III) PCO activity was higher in the mixed suspensions (regardless of the mixing ratio) than in pure mCN suspension. This implies that WO_3 should be involved in the activation of H_2O_2 by facilitating the regenerative cycle of Fe^{3+} to Fe^{2+} because WO_3 itself has a low activity for direct PCO of As(III) [16]. The comparison of [H_2O_2] at the irradiation time of 90 min between pure mCN and the mixture (mCN:WO_3 (60:40)) catalytic system shows that H_2O_2 generated in the mixture catalytic system is lower by 50 μM (than that in pure mCN) in the absence of As(III) and Fe^{3+} (Fig. 1a) whereas the production of As(V) in the mixture catalytic system is higher by 363 μM (than that in pure mCN) in the presence of 500 μM As(III) and 70 μM Fe^{3+} (Fig. 2). If As(III) were oxidized directly by Fe^{3+} (70 μM), only 35 μM of As(III) would be oxidized to As(V) [31]. This implies that this hybrid system based on *in-situ* generated H_2O_2 should be catalytic in the presence of WO_3 that enables a regenerative cycle between Fe^{3+} and Fe^{2+} under visible light. Since the concentrations of As(III) in groundwater are much lower [32], the visible light-induced oxidation of 10 μM As(III) was also tested under a similar condition except that the catalyst and Fe^{3+} concentrations decreased to a tenth (1.0 → 0.1 g/L; 70 → 7 μM, respectively) to rule out the adsorption effect (Fig. S10). Despite the much lower catalyst concentration, the mixture catalytic system still showed a better performance in oxidizing 10 μM As(III) than mCN or WO_3 alone.

3.3. Proposed mechanism for arsenic oxidation

To confirm the role of H_2O_2 as a main oxidant of As(III), the photocatalytic formation of H_2O_2 and the concurrent production of As(V) were monitored simultaneously in the optimized catalyst mixture (mCN:WO_3 (60:40)) in the absence and presence of Fe^{3+} (Fig. 3). The presence of Fe^{3+} markedly accelerated the As(III) PCO rate with maintaining the concentration of H_2O_2 low. On the other hand, the absence of Fe^{3+} significantly retarded the As(III) PCO rate while accumulating higher concentrations of H_2O_2. This confirms that *in-situ* generated H_2O_2 was consumed as an oxidant of As(III) via Fenton reaction.

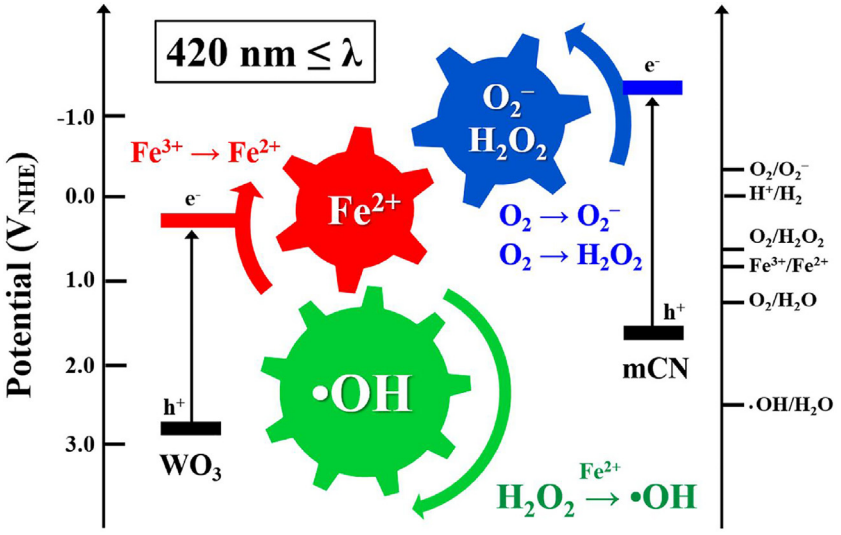

Scheme 1. Schematic diagram for possible charge transfer pathways on mCN and WO_3 in the presence of Fe^{3+}.

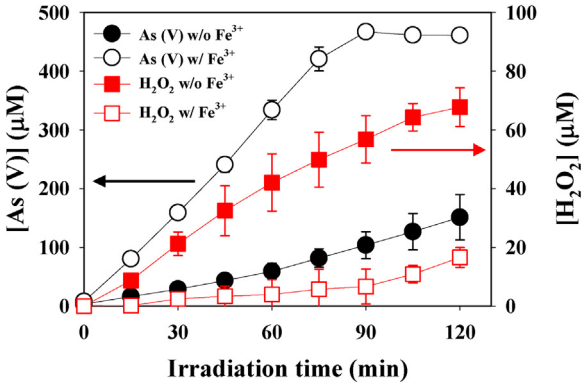

Fig. 3. Time profiles of the concurrent production of As(V) and H_2O_2 in the optimized catalyst mixture (mCN:WO_3 (60:40)) in the presence and absence of Fe^{3+}.

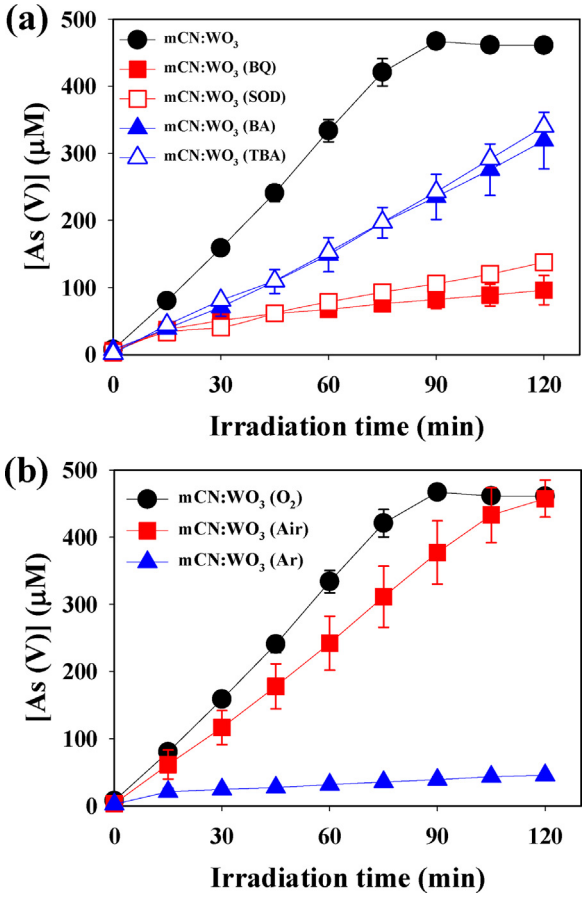

Fig. 4. (a) Photocatalytic oxidation of As(III) to As(V) in the optimized catalyst mixture (mCN:WO_3 (60:40)) with Fe^{3+} in the presence of superoxide scavengers (BQ and SOD) or OH radical scavengers (TBA and BA). 20 mM BQ, 0.125 mg/mL SOD, 500 mM TBA, and 20 mM BA. (b) Photocatalytic oxidation of As(III) to As(V) under air, Ar, and O_2-saturated conditions in the optimized catalyst mixture (mCN:WO_3 (60:40)) with Fe^{3+}. Experimental conditions for (a) and (b): [cat.] = 1.0 g/L, $[As(III)]_0$ = 500 μM, $[Fe^{3+}]$ = 70 μM, pH_i = 3, and λ > 420 nm.

Previous studies on As(III) PCO proposed that superoxide anions, hydroxyl radicals, and holes can participate in the oxidation of As(III), depending on the experimental conditions [10,33–38]. Fig. 4a shows that the PCO rate of As(III) was significantly reduced by the addition of excessive benzoquinone (BQ) or superoxide dismutase (SOD) as a superoxide scavenger, which indicates that the superoxide is involved in the oxidation of As(III). The scavenging of superoxide should inhibit the formation of H_2O_2 as well and, as a result, the formation of hydroxyl radicals should be also hindered. The remaining PCO activity in the presence of BQ or SOD is ascribed largely to the hole-mediated oxidation. On the other hand, when excess *tert*-butyl alcohol (TBA) or benzoic acid (BA) was added as a hydroxyl radical scavenger, it also markedly retarded the PCO rate. The result of the scavenger tests implies that both superoxide and hydroxyl radical are involved as a main oxidant of As(III) in this visible light-induced PCO system [10].

To investigate the role of dissolved oxygen in the PCO of As(III), the PCO activities of the optimized catalyst mixture (mCN:WO_3 (60:40)) were measured and compared in air-, O_2^-, and Ar-saturated suspensions (Fig. 4b). The PCO rate was negligibly slow under Ar saturation. However, the PCO rate was greatly accelerated in the O_2^- and air-saturated condition and was higher under O_2 saturation than air saturation, which indicates that the dissolved O_2 is an essential precursor of the oxidant responsible for the conversion of As(III) → As(V). This is consistent with the above discussion that in-situ generated superoxide and H_2O_2 from O_2 reduction are mainly responsible for the efficient oxidation of As(III).

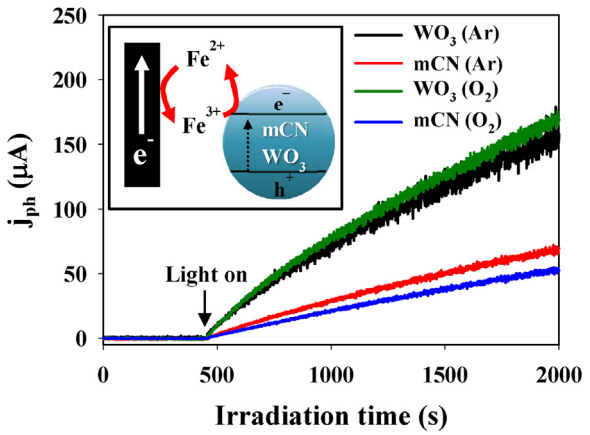

Fig. 5. Fe^{3+}-mediated photocurrent collected on a Pt electrode in mCN and WO_3 suspensions under Ar- and O_2-saturated condition. The inset shows the current collection on a Pt electrode immersed in an visible light-illuminated mCM or WO_3 suspension. Experimental conditions: [cat.] = 1.0 g/L, [Fe^{3+}] = 1 mM, pH_i = 1.7, λ > 420 nm, [$NaClO_4$] = 1 mM, Pt electrode held at +0.7 V (*vs.* Ag/AgCl).

3.4. Photo-induced interfacial charge transfer

The interfacial electron transfer from the photocatalyst surface to dissolved O_2 molecule can be indirectly monitored by measuring the photocurrent collected by the $Fe^{3+/2+}$ electron shuttle in the irradiated catalyst suspension under O_2^- or Ar-saturation [39]. As shown in Fig. 5, the time profile of the Fe^{3+}-mediated photocurrent generation was little affected by the presence of dissolved O_2 in WO_3 suspension. This clearly indicates that the CB electron transfer to Fe^{3+} is facile on WO_3 whereas the CB electron transfer to O_2 on WO_3 is insignificant. This is also consistent with the observation that no H_2O_2 was produced in pure WO_3 suspension under visible light. On the other hand, the Fe^{3+}-mediated photocurrent generation was moderately reduced in the presence of O_2 in mCN suspension, which implies that the CB electrons on mCN can transfer to both Fe^{3+} and O_2 [29]. In addition, the comparison of the Fe^{3+}-mediated photocurrent generation between mCN and WO_3 suspensions under the same experimental condition shows that the visible light-induced CB electron transfer to Fe^{3+} is far more efficient on WO_3 than on mCN. This indicates that the main role of WO_3 is to facilitate the conversion of Fe^{3+} to Fe^{2+}. Since Fe^{3+} should be continuously regenerated to effectively activate H_2O_2 in Fenton reaction, the electron transfer to Fe^{3+} involved in the presence of photocatalyst [40], electrocatalyst [41], and carbon materials [42] determines the overall oxidation kinetics. The PCO activity of As(III) was optimized at a specific mixing ratio (mCN:WO_3 = 60:40), which implies that there is an optimal balance between the CB electron transfer to dissolved O_2 (to produce H_2O_2 on mCN) and that to Fe^{3+} (to regenerate Fe^{2+} on WO_3).

4. Conclusions

The physically-mixed suspension of mCN and WO_3 in the presence of Fe^{3+} shows a highly enhanced photoactivity for the oxidation of As(III) under visible light irradiation without using noble metal catalysts and chemical additives. It is proposed that this hybrid photocatalytic system operates on the basis of in-situ generation of superoxide and H_2O_2 via O_2 reduction and the subsequent Fenton reaction. H_2O_2 is produced mainly by mCN part and the regenerative cycle of Fe^{3+}/Fe^{2+} is mainly driven by the WO_3 part. As a result of the competing dual functions of mCN and WO_3, the overall photocatalytic activity was optimized at a specific mixing ratio of two heterogeneous catalysts. The overall mechanism is schematically illustrated in Scheme 1. Finally, it should be mentioned that the present catalytic system consists of earth abundant elements only and operates with utilizing visible light photons and dissolved O_2 only, which is intrinsically eco-friendly and cost effective.

Acknowledgements

This research was financially supported by the Global Research Laboratory (GRL) Program (No. NRF-2014K1A1A2041044), Basic Science Research Program (NRF-2017R1A2B2008952), and KCAP (Sogang Univ.) (No. 2009-0093880), which were funded by the Korea Government (MSIP) through the National Research Foundation of Korea (NRF).

Appendix A. Supplementary data

Supplementary data associated with this article can be found, in the online version, at http://dx.doi.org/10.1016/j.apcatb.2017.07.021.

References

[1] D.K. Nordstrom, Public health worldwide occurrences of arsenic in ground water, Science 296 (2002) 2143–2145.
[2] E.G. Duncan, W.A. Maher, S.D. Foster, Contribution of arsenic species in unicellular algae to the cycling of arsenic in marine ecosystems, Environ. Sci. Technol. 49 (2015) 33–50.
[3] D.J. Carlin, M.F. Naujokas, K.D. Bradham, J. Cowden, M. Heacock, H.F. Henry, J.S. Lee, D.J. Thomas, C. Thompson, E.J. Tokar, M.P. Waalkes, L.S. Birnbaum, W.A. Suk, Arsenic and environmental health: state of the science and future research opportunities, Environ. Health Perspect. 124 (2016) 890–899.
[4] A. Sarkar, B. Paul, The global menace of arsenic and its conventional remediation—a critical review, Chemosphere 158 (2016) 37–49.
[5] G. Jegadeesan, S.R. Al-Abed, V. Sundaram, H. Choi, K.G. Scheckel, D.D. Dionysiou, Arsenic sorption on TiO_2 nanoparticles: size and crystallinity effects, Water Res. 44 (2010) 965–973.
[6] Y. Si, G. Li, F. Zhang, Energy-efficient oxidation and removal of arsenite from groundwater using air-cathode iron electrocoagulation, Environ. Sci. Technol. Lett. 4 (2017) 71–75.
[7] Arsenic Treatment Technology Evaluation Handbook for Small Systems, E.P. Agency, Washington, DC, 2003.
[8] L.W. Gill, C. O'Farrell, Solar oxidation and removal of arsenic—key parameters for continuous flow applications, Water Res. 86 (2015) 46–57.
[9] H. Park, H.I. Kim, G.H. Moon, W. Choi, Photoinduced charge transfer processes in solar photocatalysis based on modified TiO_2, Energy Environ. Sci. 9 (2016) 411–433.
[10] G. Moon, D.H. Kim, H.I. Kim, A.D. Bokare, W. Choi, Platinum-like behavior of reduced graphene oxide as a cocatalyst on TiO_2 for the efficient photocatalytic oxidation of arsenite, Environ. Sci. Technol. Lett. 1 (2014) 185–190.
[11] V. Vaiano, G. Iervolino, D. Sannino, L. Rizzo, G. Sarno, A. Farina, Enhanced photocatalytic oxidation of arsenite to arsenate in water solutions by a new catalyst based on MoOx supported on TiO_2, Appl. Catal. B—Environ. 160 (2014) 247–253.
[12] Q. Li, N.J. Easter, J.K. Shang, As(III) removal by palladium-modified nitrogen-doped titanium oxide nanoparticle photocatalyst, Environ. Sci. Technol. 43 (2009) 1534–1539.
[13] L.Y. Xie, P. Liu, Z.Y. Zheng, S.X. Weng, J.H. Huang, Morphology engineering of V_2O_5/TiO_2 nanocomposites with enhanced visible lightle-driven photofunctions for arsenic removal, Appl. Catal. B—Environ. 184 (2016) 347–354.
[14] J. Hu, S.X. Weng, Z.Y. Zheng, Z.X. Pei, M.L. Huang, P. Liu, Solvents mediated-synthesis of BiOI photocatalysts with tunable morphologies and their visible-light driven photocatalytic performances in removing of arsenic from water, J. Hazard. Mater. 264 (2014) 293–302.
[15] Q.F. Tian, J.D. Zhuang, J.X. Wang, L.Y. Xie, P. Liu, Novel photocatalyst $Bi_2Sn_2O_7$, for photooxidation of As(III) under visible-light irradiation, Appl. Catal. A—Gen. 425 (2012) 74–78.
[16] J. Kim, C.W. Lee, W. Choi, Platinized WO_3 as an environmental photocatalyst that generates OH radicals under visible light, Environ. Sci. Technol. 44 (2010) 6849–6854.
[17] G. Moon, W. Kim, A.D. Bokare, N.E. Sung, W. Choi, Solar production of H_2O_2 on reduced graphene oxide-TiO_2 hybrid photocatalysts consisting of earth-abundant elements only, Energy Environ. Sci. 7 (2014) 4023–4028.
[18] Y. Shiraishi, S. Kanazawa, Y. Kofuji, H. Sakamoto, S. Ichikawa, S. Tanaka, T. Hirai, Sunlight-driven hydrogen peroxide production from water and molecular oxygen by metal-free photocatalysts, Angew. Chem.—Int. Edit. 53 (2014) 13454–13459.
[19] G. Moon, M. Fujitsuka, S. Kim, T. Majima, X. Wang, W. Choi, Eco-friendly photochemical production of H_2O_2 through O_2 reduction over carbon nitride

frameworks incorporated with multiple heteroelements, ACS Catal. 7 (2017) 2886–2895.
[20] Y. Shiraishi, S. Kanazawa, Y. Sugano, D. Tsukamoto, H. Sakamoto, S. Ichikawa, T. Hirai, Highly selective production of hydrogen peroxide on graphitic carbon nitride (g-C_3N_4) photocatalyst activated by visible light, ACS Catal. 4 (2014) 774–780.
[21] S. Chu, Y. Wang, Y. Guo, J.Y. Feng, C.C. Wang, W.J. Luo, X.X. Fan, Z.G. Zou, Band structure engineering of carbon nitride: in search of a polymer photocatalyst with high photooxidation property, ACS Catal. 3 (2013) 912–919.
[22] V. Maurino, C. Minero, G. Mariella, E. Pelizzetti, Sustained production of H_2O_2 on irradiated TiO_2 – fluoride systems, Chem. Commun. (2005) 2627–2629.
[23] M. Teranishi, S. Naya, H. Tada, In situ liquid phase synthesis of hydrogen peroxide from molecular oxygen using gold nanoparticle-loaded titanium(IV) dioxide photocatalyst, J. Am. Chem. Soc. 132 (2010) 7850–7851.
[24] S.N. Li, G.H. Dong, R. Hailili, L.P. Yang, Y.X. Li, F. Wang, Y.B. Zeng, C.Y. Wang, Effective photocatalytic H_2O_2 production under visible light irradiation at g-C_3N_4 modulated by carbon vacancies, Appl. Catal. B—Environ. 190 (2016) 26–35.
[25] G. Longobucco, L. Pasti, A. Molinari, N. Marchetti, S. Caramori, V. Cristino, R. Boaretto, C.A. Bignozzi, Photoelectrochemical mineralization of emerging contaminants at porous WO_3 interfaces, Appl. Catal. B—Environ. 204 (2017) 273–282.
[26] D.T. Sawyer, J.S. Valentine, How super is superoxide? Acc. Chem. Res. 14 (1981) 393–400.
[27] E.A. Meulenkamp, Mechanism of WO_3 electrodeposition from peroxy-tungstate solution, J. Electrochem. Soc. 144 (1997) 1664–1671.
[28] K. Ishibashi, A. Fujishima, T. Watanabe, K. Hashimoto, Detection of active oxidative species in TiO_2 photocatalysis using the fluorescence technique, Electrochem. Commun. 2 (2000) 207–210.
[29] J. Schwitzgebel, J.G. Ekerdt, H. Gerischer, A. Heller, Role of the oxygen molecule and of the photogenerated electron in TiO_2-photocatalyzed air oxidation reactions, J. Phys. Chem. 99 (1995) 5633–5638.
[30] S. Nakade, T. Kanzaki, W. Kubo, T. Kitamura, Y. Wada, S. Yanagida, Role of electrolytes on charge recombination in dye-sensitized TiO_2 solar cell (1): the case of solar cells using the I^-/I_3^- redox couple, J. Phys. Chem. B 109 (2005) 3480–3487.
[31] S.J. Hug, O. Leupin, Iron-catalyzed oxidation of arsenic(III) by oxygen and by hydrogen peroxide: pH-dependent formation of oxidants in the Fenton reaction, Environ. Sci. Technol. 37 (2003) 2734–2742.
[32] R. Nickson, J. McArthur, W. Burgess, K.M. Ahmed, P. Ravenscroft, M. Rahman, Arsenic poisoning of Bangladesh groundwater, Nature 395 (1998) 338.
[33] J. Ryu, W. Choi, Effects of TiO_2 surface modifications on photocatalytic oxidation of arsenite: the role of superoxides, Environ. Sci. Technol. 38 (2004) 2928–2933.
[34] J. Ryu, W.Y. Choi, Photocatalytic oxidation of arsenite on TiO_2: understanding the controversial oxidation mechanism involving superoxides and the effect of alternative electron acceptors, Environ. Sci. Technol. 40 (2006) 7034–7039.
[35] J. Kim, G.H. Moon, S. Kim, J. Kim, Photocatalytic oxidation mechanism of arsenite on tungsten trioxide under visible light, J. Photochem. Photobiol. A—Chem. 311 (2015) 35–40.
[36] W. Choi, J. Yeo, J. Ryu, T. Tachikawa, T. Majima, Photocatalytic oxidation mechanism of As(III) on TiO_2: unique role of As(III) as a charge recombinant species, Environ. Sci. Technol. 44 (2010) 9099–9104.
[37] P.K. Dutta, S.O. Pehkonen, V.K. Sharma, A.K. Ray, Photocatalytic oxidation of arsenic(III): Evidence of hydroxyl radicals, Environ. Sci. Technol. 39 (2005) 1827–1834.
[38] T.L. Xu, P.V. Kamat, K.E. O'Shea, Mechanistic evaluation of arsenite oxidation in TiO_2 assisted photocatalysis, J. Phys. Chem. A 109 (2005) 9070–9075.
[39] H. Park, W. Choi, Photoelectrochemical investigation on electron transfer mediating behaviors of polyoxometalate in UV-illuminated suspensions of TiO_2 and Pt/TiO_2, J. Phys. Chem. B 107 (2003) 3885–3890.
[40] H. Lee, J. Choi, S. Lee, S.T. Yun, C. Lee, J. Lee, Kinetic enhancement in photocatalytic oxidation of organic compounds by WO_3 in the presence of Fenton-like reagent, Appl. Catal. B—Environ. 138 (2013) 311–317.
[41] Z.M. Qiang, J.H. Chang, C.P. Huang, Electrochemical regeneration of Fe^{2+} in Fenton oxidation processes, Water Res. 37 (2003) 1308–1319.
[42] Y.X. Qin, L.Z. Zhang, T.C. An, Hydrothermal carbon-mediated fenton-like reaction mechanism in the degradation of alachlor: direct electron transfer from hydrothermal carbon to Fe(III), ACS Appl. Mater. Interfaces 9 (2017) 17116–17125.